Geologie en Mijnbouw **77:** 177–188, 1999.

Background of ground-penetrating radar measurements

J. van der Kruk, E.C. Slob & J.T. Fokkema
Section of Applied Geophysics, Subfaculty of Applied Earth Sciences, Faculty of Civil Engineering and Geosciences, Delft University of Technology, Mijnbouwstraat 120, 2600 GA, Delft, the Netherlands

Received 3 March 1997; accepted in revised form 17 December 1998

Key words: field surveys, GPR

Abstract

Characterization of the shallow subsurface (0.25 to 10 m) is of growing importance for engineering activities, solutions of environmental problems, and archaeological investigations. Ground-penetrating radar (GPR) is an appropriate technique considering the depth range of interest, the strength of electric and magnetic contrasts between different subsurface layers and buried objects, and the required resolution. GPR surveys can detect subsurface structures by recording electromagnetic reflections from discontinuities. The detectability of objects and the delineation of subsurface structures increases with increasing wave velocity and conductivity differences between the object and its surroundings or between adjacent layers. However, unwanted reflections from objects above the surface influence the images. Shielded antennas can be used to avoid strong reflections from these objects. The data thus obtained are, however, more difficult to interpret. The fundamentals of GPR and two different acquisition setups for a GPR system are discussed. Basic interpretation tools for travel-time and velocity estimation are described, and finally, case studies are presented, followed by conclusions.

Basic principles

A ground-penetrating radar (GPR) system uses a transmitting antenna, which emits an electromagnetic wave field into the ground, and a receiving antenna, that records this field and its reflections from the subsurface. When an electromagnetic wave propagates through the ground and encounters a surface where the electric and/or magnetic properties of the ground change, part of its energy will be reflected and part of it will be transmitted. The Maxwell equations give a mathematical description of the propagation, reflection and transmission of electromagnetic fields. In these equations, the electric and magnetic fields are coupled vector fields. An extensive mathematical treatment of the theory of electromagnetic fields can be found in Felsen & Markowitz (1994) and De Hoop (1995), whereas typical electric and magnetic properties for geological materials can be found in Davis & Annan (1989). The propagation velocity of an electromagnetic wave in a medium is determined by the electric permittivity (ϵ), and the magnetic permeability (μ), while the part of the kinetic energy that is irreversibly converted into heat is determined by the electric conductivity (σ). In a homogeneous medium, both the electric and magnetic fields can be described in terms of the scalar function:

$$\hat{G}(R,\omega) = \frac{\exp(-\gamma R)}{4\pi R}, \tag{1}$$

where ω denotes the radial frequency of operation and R denotes the radial distance from the source. The function is known as the Green function. The amplitude/phase factor γ is given by:

$$\gamma = j\frac{\omega}{c}\left(1 - j\frac{\sigma}{\omega\epsilon}\right)^{1/2} = j\frac{\omega}{v(\omega)} + \alpha(\omega)$$
$$\text{with } \mathrm{Re}\{\gamma\} \geq 0, \tag{2}$$

where $\mathrm{Re}\{\gamma\}$ is the real part of γ and j is the imaginary unit: $j^2 = -1$. The imaginary part of γ is related to the

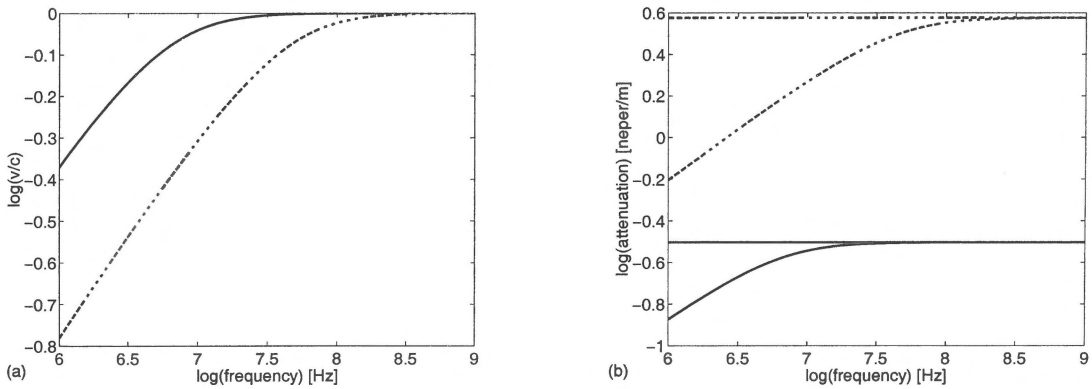

Figure 1. Log-log plot of phase velocities normalized to the corresponding wave velocities (a), and the attenuation factors together with their high-frequency asymptotes (b), for a dry sandy subsoil model with a relative electric permittivity of 9 and a conductivity of 5 mS/m (solid lines), and a water-saturated sandy soil model with with a relative electric permittivity of 25 and a conductivity of 100 mS/m (dashed lines).

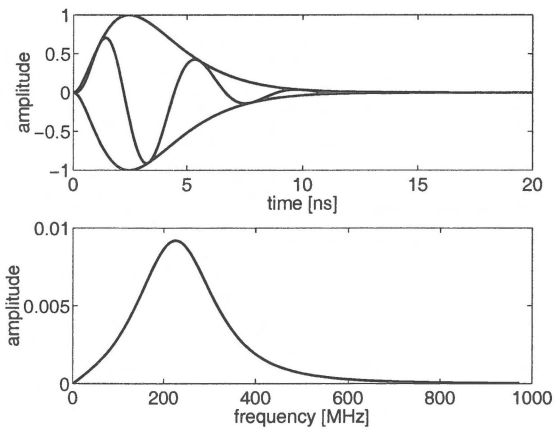

Figure 2. The time behaviour and the amplitude spectrum of an amplitude-modulated sine as a good approximation of an actual GPR source pulse. Its center frequency is $f_c = 225$ MHz.

travel time of the wave from a source to a receiver, while the real part of γ is related to the amount of energy that is converted into heat on that trajectory. In the above formula, $v(\omega)$ is known as the, frequency-dependent, phase velocity, while $\alpha(\omega)$ is known as the, frequency-dependent, attenuation factor. The exact arrival time of the wave is determined by the high-frequency limit of the phase velocity, which is equal to the wave velocity, c. In the high-frequency limit, the attenuation factor becomes independent of frequency, and the phase attenuation factor is given by:

$$\gamma \overset{\omega\to\infty}{=} j\frac{\omega}{c} + \frac{1}{2}Z\sigma, \tag{3}$$

where $Z = \sqrt{\mu/\epsilon}$ is the wave impedance. GPR performs well in the frequency range where the displacements currents are dominant, i.e. in an environment with relatively small energy losses ($\sigma \ll \omega\epsilon$). In these situations the pulse is damped on its propagation path but the pulse shape is not distorted. However, in case of a high-contrast shallow subsoil, which is typical for the Netherlands situation, a joint diffusion and wave propagation occurs. In these types of subsurface, both attenuation of, and changes in the pulse shape take place (Annan 1996). Figure 1 shows the phase velocity normalized to the corresponding wave velocity and the attenuation factor with its high-frequency asymptotic value, respectively, as a function of frequency on a log-log scale. In this figure, the solid lines represent a dry sandy soil (subsurface) with a relative electric permittivity of 9 and a conductivity of 5 mS/m while dashed lines represent a water-saturated soil (subsurface) with a relative electric permittivity of 25 and a conductivity of 100 mS/m. These two (sub)soil models are used for all examples in this section and are referred to as dry soil and wet soil, respectively. Velocity dispersion of the signal occurs when the phase velocity is different from the wave velocity. For the dry soil this occurs for GPR antennas with a center frequency up to about 30 MHz and for the water-saturated soil this occurs for GPR antennas with a center frequency up to about 300 MHz. For antennas with a higher center frequency, there is no velocity dispersion. Attenuation dispersion occurs where the attenuation factor is different from its high-frequency limit. For the two examples shown, this occurs for GPR antennas with center frequencies up to about 30 and 300 MHz, respectively. Note that the conductivity ratio between the wet and dry soil is

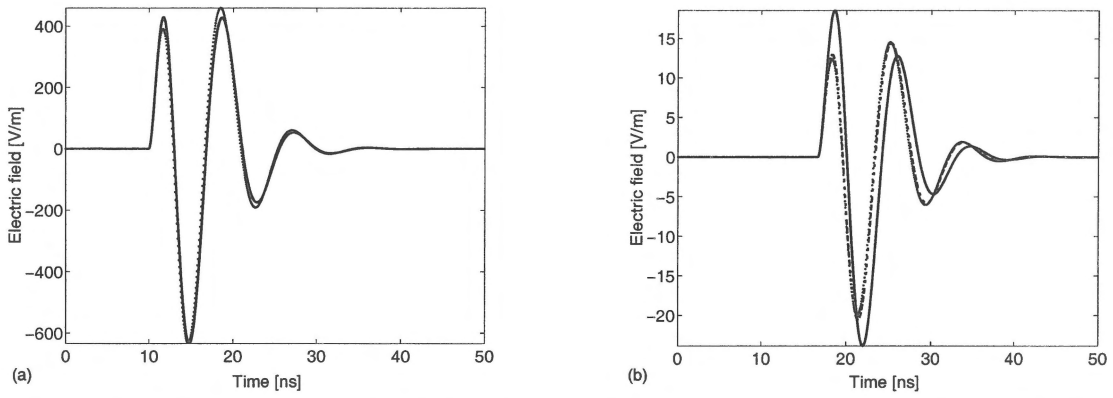

Figure 3. The electric field after propagating 1 m through the dry subsoil (a) and the wet subsoil (b). Solid lines represent the actual field, dashed lines the field in the high-frequency approximation, while the dotted lines represent the field in the scalar far-field approximation in the high-frequency approximation.

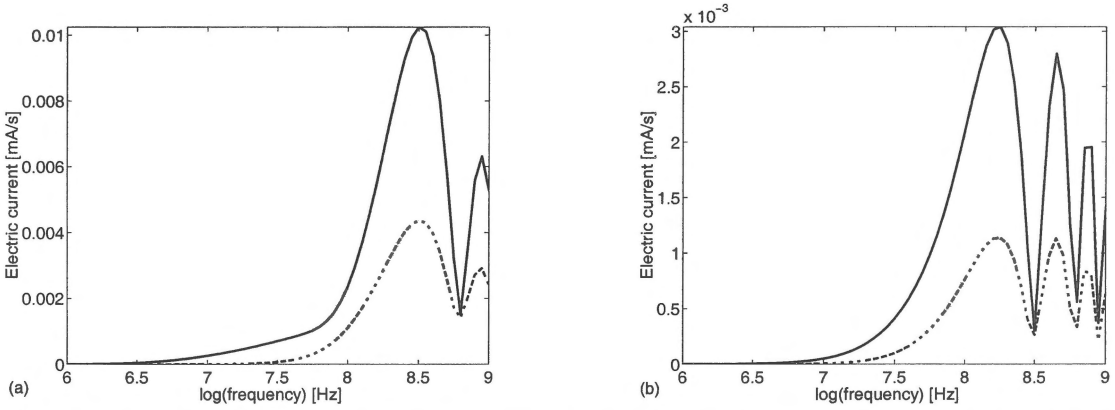

Figure 4. Illustration of the differences between the electric current in a receiver antenna modeled as an electric dipole of finite length. The antenna is placed at the earth surface of the dry subsoil model (a) and the wet subsoil model (b). The solid lines correspond to the actual current and the dashed lines to the current obtained using the scalar far-field approximation. The length of both source and receiver antennas is 25 cm, and the distance between them is also 25 cm, while they are placed parallel to each other. This corresponds to a 450 MHz antenna.

20, while the ratio of the attenuation factors is 12. This is because the attenuation is not a function of the conductivity alone, but of the ratio between the conductivity and the square root of the relative permittivity, as can be seen from the high-frequency limit of the attenuation factor.

Electromagnetic fields are vector fields and electric sources are vectors also. A GPR source antenna emits a time pulse, with a usually small frequency band around a specified center frequency, f_c, into the ground. A good model of such a pulse is an amplitude-modulated sine, which resembles actual recordings very well. An example is given for a center frequency of 225 MHz, in Figure 2, where the time pulse is shown with its envelope (top) and its corresponding frequency spectrum (bottom). The electric field component parallel to the direction of the source, contains a scalar term and a polarization term. The electric field components normal to the direction of the source only contain polarization terms. These polarization terms contain terms proportional to (R^{-3}), the near-field, proportional to (R^{-2}), the intermediate-field, and proportional to (R^{-1}), the far-field. The scalar term only has a far-field contribution. In the usual GPR set-up the source and receiver antennas are placed parallel to each other on the earth surface. If we neglect the size of the antennas, then the far-field contribution only comes from the scalar term. But the total electric field at the receiver also has near-field and intermediate-field terms. In the literature, the high-frequency, scalar far-field approximation is mostly used, see e.g. Fisher al. (1992), Turner

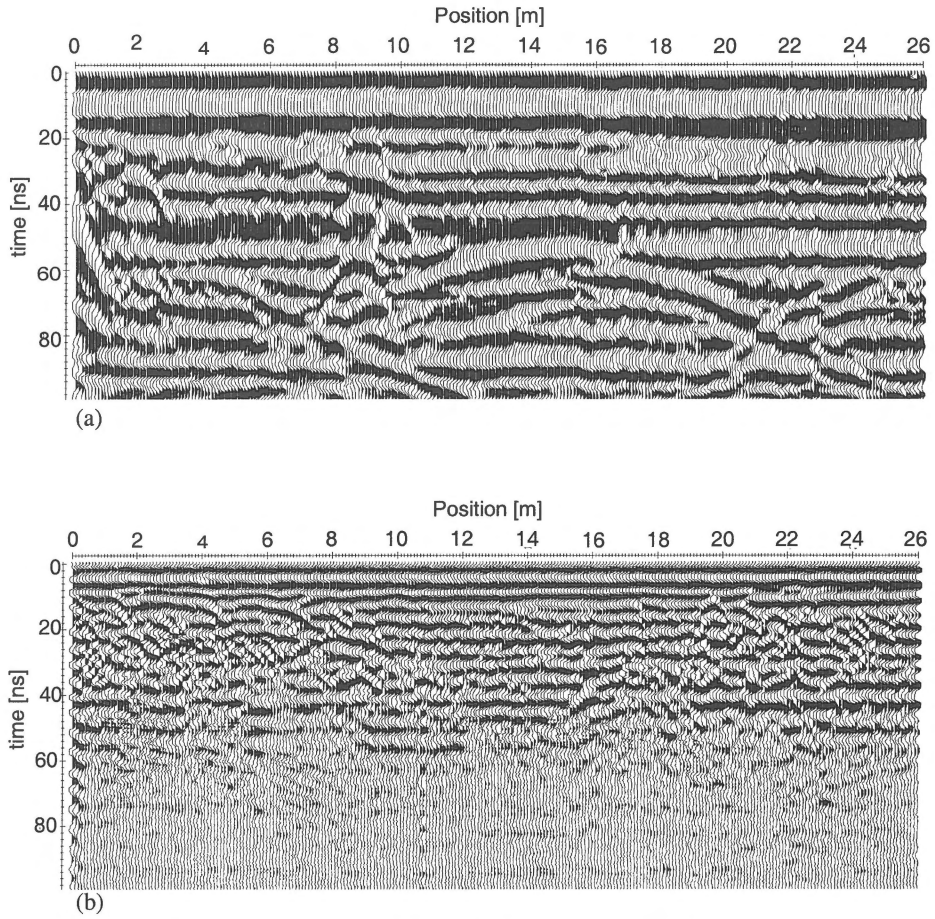

Figure 5. Radargram of a survey line carried out on a field with trees with 200 MHz unshielded antennas (a) and 225 MHz shielded antennas (b). The trees are aligned parallel to the survey line. The reflection patterns of the trees are clearly visible in (a) as hyperbolas arriving later than 50 ns, while in (b) they are hardly visible.

(1994) and Goodman (1994). Figure 3 shows for the dry and wet model soils the accuracy of the far-field approximation for two different antennas. In this figure, the exact field (i.e. the field computed without any approximation) is plotted together with the field that results from the high-frequency approximation and the field that results from only the far-field term in the high-frequency approximation. The latter is the most commonly used approximation for modeling and data processing for GPR applications. In Figure 3, the distance between the source and the receiver is 1 m, which is the practical distance in a normal field survey with a 100 MHz antenna. For the dry soil (Figure 3a) the high-frequency approximation lies on top of the exact result, while the far-field term of the high-frequency approximation is off by less than 10% in the positive amplitude peaks. For the wet soil (Figure 3b) the far-field approximation in itself is good but the high-frequency approximation is not. The effects of velocity and phase dispersion are clearly visible in the amplitude differences in the first and second positive peaks and in the timing of the peaks. From Figures 1 and 3 we infer that for both these models the scalar far-field high-frequency approximation will be reasonably accurate for antennas with a center frequency higher than 200 MHz.

With both the source and the receiver antennas at the earth surface, two waves travel directly from source to receiver; one at the speed of light through the air along the surface and the other through the ground along the surface at a speed, which is determined by the electric permittivity and magnetic permeability of the soil close to the surface. We have modeled the GPR antennas as electric dipoles of finite lengths. The

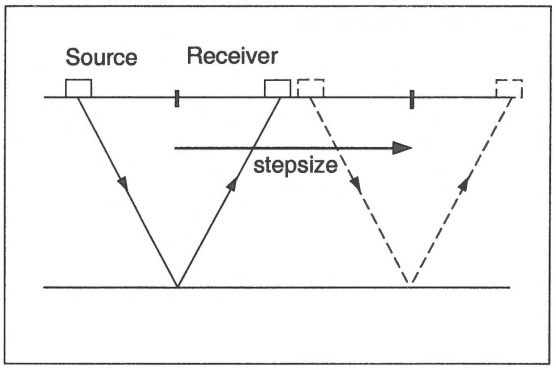

Figure 6. Common-offset configuration for GPR where the source and receiver are at a fixed distance and they are moved together for each measurement.

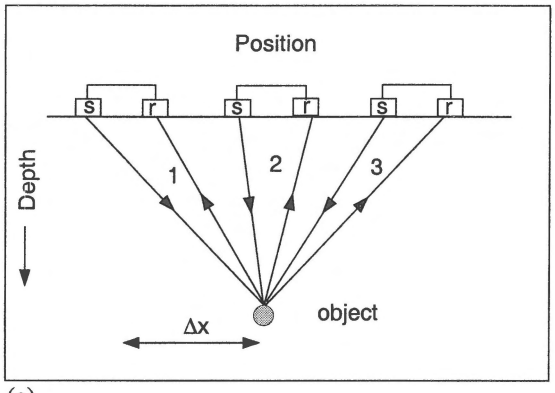

(a)

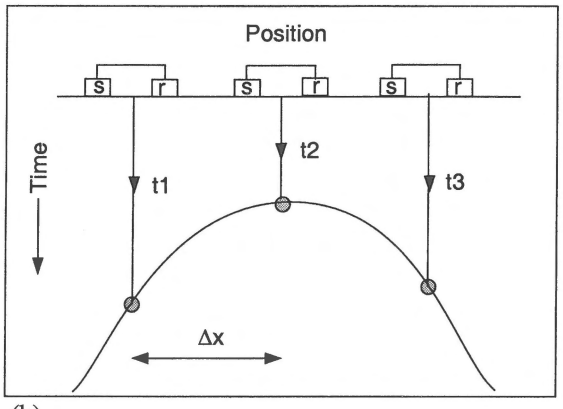

(b)

Figure 7. The shortest travel paths for waves from transmitter (s) to an object and back to receiver (r) at different positions of the antennas on the surface in a common-offset survey (a), lead to a hyperbolic event in time as a function of the position of the antennas (b). From this event the velocity of the waves travelling in the subsoil between the surface and the object can be estimated.

source antenna is excited by applying a voltage time pulse and we compute the current that is generated in the wire. Then we use the computed current as the electric source and compute the field that is emitted from the antenna to the receiving antenna. This field generates a current in the receiving antenna and is recorded by the recording device attached to the antenna. We have used the actual field to compute the field from source antenna to receiver antenna and also used the scalar far-field approximation. To compute the currents in the antennas we have used the expressions containing near-field, intermediate-field and far-field terms, since they are all important inside the antenna. So in the case where we have used the scalar far-field approximation, we have only used the approximation to compute the field from the source to the receiver. Figures 4a and b show the results for the dry and wet soils, respectively, in the receiver antenna as a function of frequency from 1 MHz to 1 GHz. The length of the antennas is 25 cm and their distance is also 25 cm. This corresponds to the set-up of a 450 MHz antenna. It is observed that in both cases the vectorial character of the GPR problem cannot be neglected for electric dipole antennas. This is due to their finite lengths. Of course, this is mostly an amplitude problem and to a lesser extent a pulse-shape problem; the timing of events, however, is correctly modeled by the far-field approximation. The onset of the signal will come at the correct time, but the peak amplitude of the signal will not be at the correct time. For velocity estimation the peak amplitude is used because the pulse onset is difficult to determine; hence, one has to be careful when using the scalar far-field approximation for velocity estimation from data.

Above-surface reflections have lost energy due to spherical spreading of the wave in air and due to the reflection itself; only perfect conductors give a perfect reflection. Subsurface reflections have lost energy due to the same reasons and usually also due to attenuation on their propagation path through a conductive ground. It is usually difficult to identify reflections in the data as above-surface reflections. To circumvent this difficulty, shielded antennas have been designed. These antennas are covered with a box containing material that damp out electromagnetic waves without causing reflections. The shielding is never perfect but usually satisfactorily suppresses above-surface reflections. An example of a survey on a field containing big trees is shown in Figure 5a. The data is obtained with unshielded antennas and reflections from the trees are clearly visible as the almost flat hyperbolas, indicating

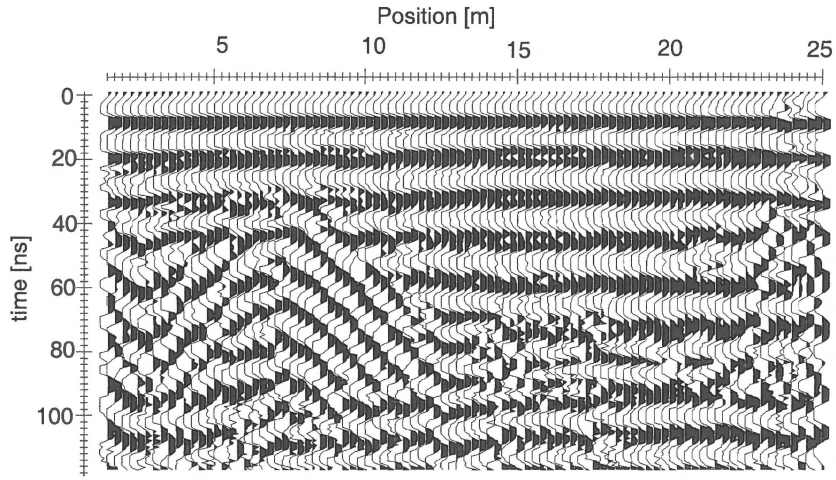

Figure 8. A real data example of the common-offset measurement with a 110 MHz antenna system where the hyperbolic event indicates the presence of an object. The distance between transmitter and receiver is 1 m, the distance between two measurements is 25 cm and the time interval between two samples is 0.7 ns. The position is depicted along the x-axis and the two-way travel time along the y-axis.

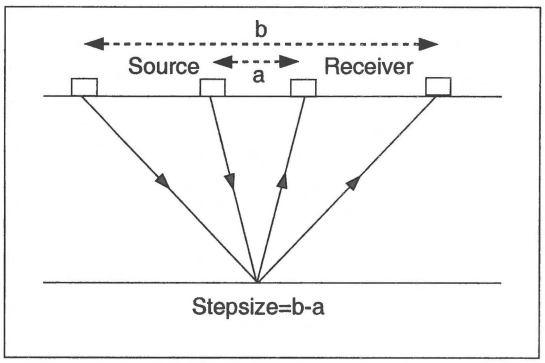

Figure 9. A schematic view of the common-midpoint configuration for GPR. The point in the middle between the source and the receiver is fixed while the source and the receiver are both moved a fixed distance away from this midpoint for each measurement.

reflections from objects in a high velocity medium. Data obtained over the same survey line with shielded antennas are shown in Figure 5b; reflections from the trees are almost absent.

Acquisition setup and velocity analysis

There are two common acquisition modes to conduct GPR surveys at the earth surface. The common-offset mode and the common-midpoint mode. Both modes can be used for profiling, while the common-midpoint method is most suited for velocity analysis on the data.

Common-offset measurement (profiling)

A GPR system is generally used in a common-offset configuration to detect objects or to investigate lateral and vertical changes in the subsurface. The source and receiver antennas are separated during measurement by a fixed distance, *offset*. Subsequently, the antennas are moved a fixed distance, *stepsize,* and another measurement is taken (Figure 6). This is repeated along a line. This method is fast and therefore relatively cheap. The data contain a reflection image of the surroundings of the antennas, but do not contain direct information about the velocities in the different layers or of the objects in the subsurface. Any object shows as an hyperbolic-like reflection pattern. Assuming there are no velocity changes between the surrounding material and the object, and assuming the object is small compared to the wavelength used, the reflection pattern is a perfect hyperbola. The slopes of the hyperbola tail can be used to estimate the velocity of the wave in the layer. The wave travels from the source to the object, reflects and travels back to the receiver (Figure 7). Assuming the source-receiver distance is small compared to the distance to the object, the velocity can be determined using the simple formula:

$$v = \frac{2\Delta x}{\Delta t}, \tag{4}$$

where $\Delta t = \sqrt{t_1^2 - t_2^2}$ and the factor 2 accounts for the

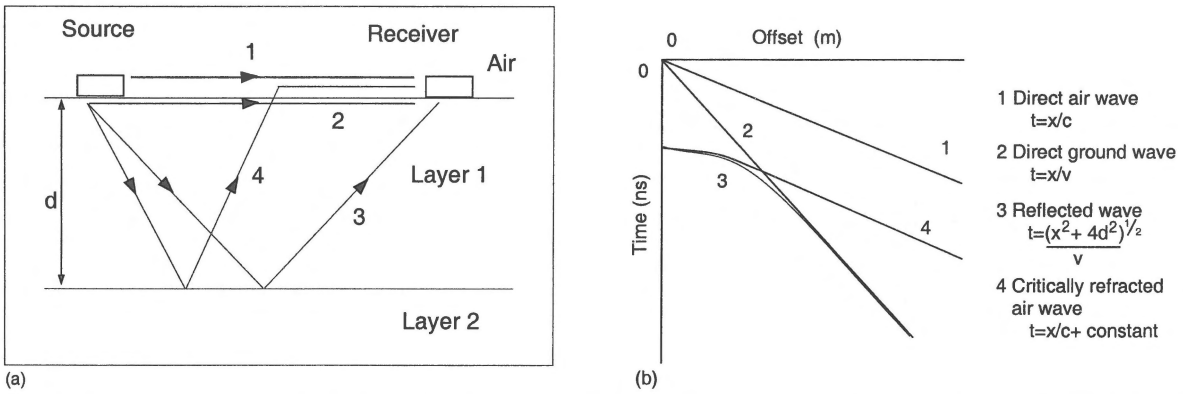

Figure 10. At a given distance between the transmitting and receiving antennas, four different waves can be distinguished if the subsoil consists of two layers that are electromagnetically different, where we assume that the wave velocity in layer 1, with thickness d, is higher than the wave velocity in layer 2. In (a) a schematic view of the shortest travelpath is given; (b) shows the correponding two-way travel times as a function of offset. Wave no. 1, the direct air-wave, travels directly from source to receiver through the air. Wave no. 2, the direct ground-wave, travels directly from source to receiver through the ground just under the earth surface. Wave no. 3, is the first reflection. Wave no. 4 occurs when the offset is so large that reflected waves at the critical angle for air arrive at the earth surface between the source and the receiver. They occur at the critical offset, which is the offset where wave no. 3 is the same as wave no. 4. At smaller offsets wave no. 4 does not travel to the receiver, while at larger offsets wave no. 4 arrives before wave no. 3 because it travels through air for some of the distance and the wave velocity in air is the largest possible velocity.

two-way travel time. An example of this is given in Figure 8 where the result of a common-offset measurement is shown for antennas with a center frequency of 110 MHz. We can estimate the velocity of the electromagnetic waves in the layer above the object from the reflection at position 7 which arrives at $t = 42.5$ ns and the reflection at position 10.5 which arrives at 67.5 ns. We then obtain:

$$v = 2\frac{10.5 - 7}{\sqrt{(67.5)^2 - (42.5)^2}} \approx 0.13\text{m/ns}. \qquad (5)$$

If there are no objects, or if the sizes of the objects are comparable to or larger than the wavelength, or if the objects are at a depth much larger than the source-receiver separation, or if the objects are not in the top layer, then it is impossible to obtain good wave-velocity estimates. In those cases the common-midpoint acquisition method is used.

Common-midpoint measurement (velocity sounding)

The velocities of layers can be obtained by the common-midpoint (CMP) measurement. The offset of both the source and receiver is increased away from a fixed midpoint. At all distances between source and receiver with a fixed midpoint, most of the energy that is reflected by, not too steeply dipping, subsurface

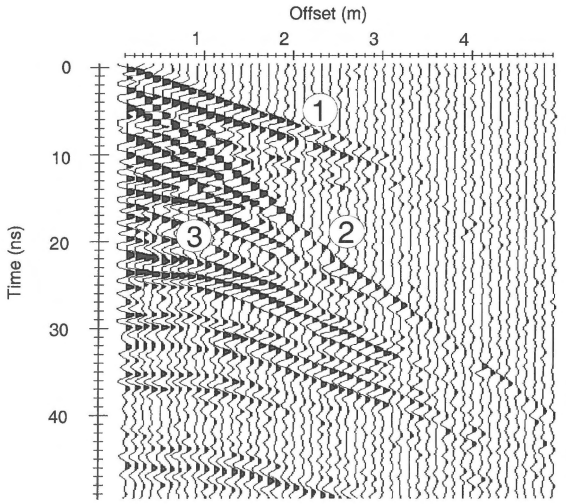

Figure 11. An example of the CMP measurement with a 900 MHz antenna system. The radargram shows the two-way travel time (y-axis) as a function of offset (x-axis). The numbered events are the direct air-wave (1), the direct ground-wave (2), and reflections from interfaces in the subsoil (3). Notice that the velocity in the ground just under the surface changes when the offset is 2.5 m, which is observed from the change in the slope of the arrival time of the ground-wave.

reflectors comes from the same points straight below that given midpoint (Figure 9). From the differences in arrival time versus offset very accurate velocity estimates can be obtained from all layers. When a CMP measurement is carried out, different events can be

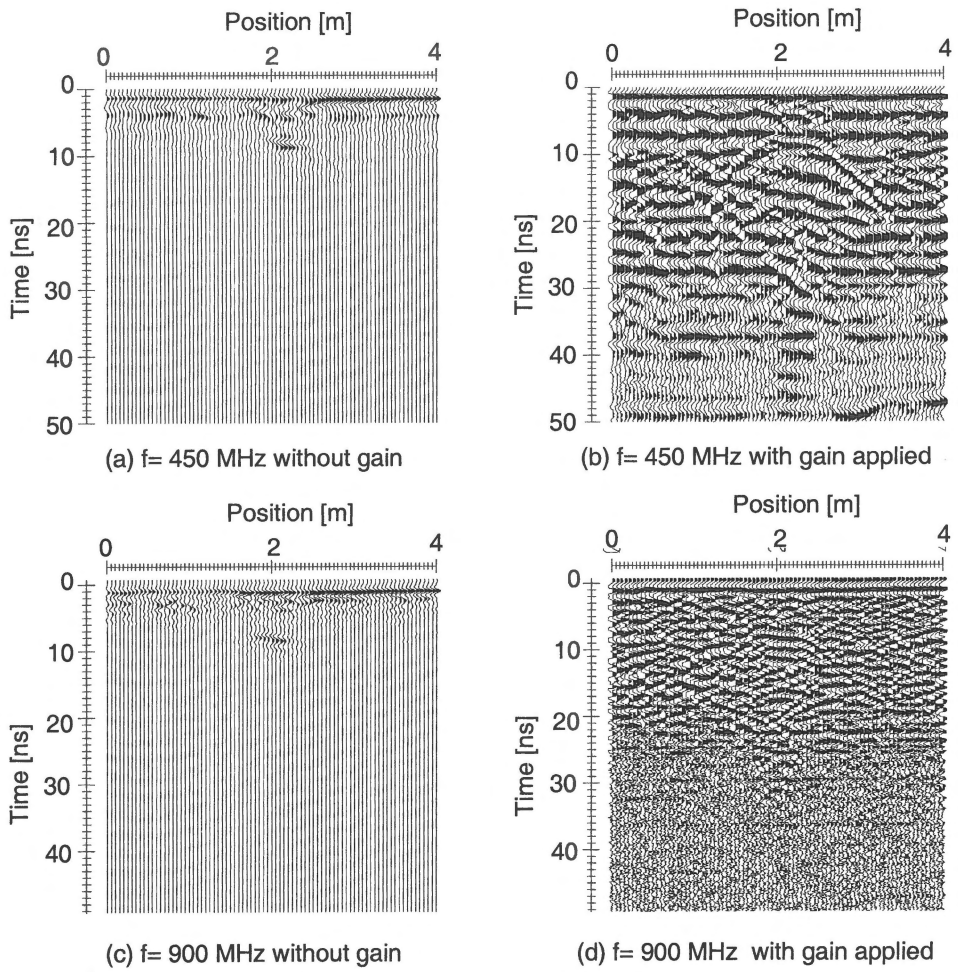

Figure 12. Detection of a steel plate using the common-offset configuration with a 450 MHz (a) and (b), and a 900 MHz antenna system (c) and (d). In (a) and (c) the data are shown at measured amplitudes, while (b) and (d) show the same data but now with a temporal gain function applied to the data. The ungained data show that a metal object can be detected without applying an amplitude gain to the data. The gained data show the diffraction hyperbolas that come from the edges of the plate, especially in the 450 MHz data. These hyperbolas are easily detected with the eye and can help in the interpretation.

distinguished in the received signal, as depicted in Figure 10a. These are the results of the air wave (1), the ground wave (2), the direct reflection from an interface (3), and the critically refracted airwave (4). Since the velocity in air is always greater than the largest velocity in the ground, a critical angle of incidence exists where the transmitted wave travels in the air along the interface. These angles only exist when the wave travels from a slower medium to a faster medium, such as a reflection from below the ground that travels toward the earth surface.

In a common-offset survey, the above mentioned events interfere and cannot be identified separately. On the other hand, in a CMP measurement they can be recognized. A theoretical result is depicted in Figure 10b. From the ground wave, we can extract the velocity of the waves just beneath the surface by determining the slope of the event, that is,

$$v = \frac{\Delta x}{\Delta t}. \tag{6}$$

The velocity can also be obtained using the first reflected wave. The velocity of which is given by:

$$v = \sqrt{\frac{b^2 - a^2}{t(b)^2 - t(a)^2}}, \tag{7}$$

where b and a denote two different offsets (Figure 9) and $t(a)$ and $t(b)$ are the corresponding two-way travel times.

The air wave (1), the ground wave (2) and a reflected wave (3), of Figure 10b are clearly visible in the experimental CMP situation depicted in Figure 11. The velocity of the air wave is

$$c = \frac{\Delta x}{\Delta t} = \frac{3 - 0.1}{9.7 - 0} = 3.0 \cdot 10^8 \text{ m/s.} \quad (8)$$

Note that this velocity almost equals that of light, by definition 299 792 458 m/s. The velocity of the ground wave is

$$v = \frac{\Delta x}{\Delta t} = \frac{2 - 0.1}{18 - 2} = 1.2 \cdot 10^8 \text{ m/s.} \quad (9)$$

The ground-wave velocity can also be determined using the first reflected wave for t = 23 ns (see Equation (7)).

$$v = \sqrt{\frac{b^2 - a^2}{t(b)^2 - t(a)^2}} \quad (10)$$
$$= \sqrt{\frac{2^2 - (0.2)^2}{28^2 - 23^2}} = 1.2 \cdot 10^8 \text{ m/s.}$$

This velocity can be used to obtain a depth indication using:

$$z = \frac{vt}{2}. \quad (11)$$

Further, the permittivity of the subsurface can be estimated, using $v = c_o/\sqrt{\epsilon_r}$, where c_o is the velocity of light in air and ϵ_r is the relative permittivity of the subsurface, a dimensionless quantity ($\epsilon = \epsilon_r \epsilon_o$). In this case the relative permittivity equals 6.25. This under the reasonable assumption that the magnetic permeability of soil equals that of free space.

Field surveys

Several GPR surveys have been carried out, which clearly demonstrate the wide range of GPR applications. Some of the surveys have been carried out under controlled circumstances and others without any prior knowledge of the subsurface. The detection of a buried steel plate and the location and environment of an abandoned mine shaft were investigated. Furthermore the influence of different subsurface properties regarding the permittivity and the conductivity have been investigated. The GPR systems used were the pulseEKKO 100 and pulseEKKO 1000 both from Sensors & Software. The pulseEKKO 100 uses unshielded antennas with center frequencies of 25, 50, 100 and 200 MHz, while the pulseEKKO 1000 uses shielded antennas with center frequencies of 110, 225, 450 and 900 MHz (Table 1).

Table 1. Acquisition parameters for the different antennas used in the field experiments.

Frequency (MHz)	System	Stepsize (m)	Sampling interval (ns)	Separation (m)
110	pE 1000	0.05	0.8	1.0
200	pE 100	0.1	0.8	0.5
225	pE 1000	0.1/0.05	0.4	0.5
450	pE 1000	0.05	0.2	0.25
900	pE 1000	0.05	0.1	0.17

Detection of a steel plate

In a low-loss environment (propagating wave regime) a steel plate was buried. The dimensions of the plate were 0.5 × 1.60 m and it was buried horizontally at a depth of 0.4 m. Measurements were carried out using center frequencies of 450 and 900 MHz. In Figure 12 the results are depicted.

Because the electric and magnetic contrasts between the iron plate and the environment are large, the plate can be detected without applying amplitude gain to the data. The diffractions at the edges of the plate are clearly visible, especially in the 450 MHz data. This is an easily recognizable feature which can help in the interpretation. From the results no conclusions can be drawn about the depth of the object, because only the travel-time is known. Therefore a CMP measurement has been carried out to obtain the velocity of the waves in the subsurface which proved to be v = 0.1 m/ns. Using Equation (11) the depth found is 0.4 m.

The first event measured (for small t) is the interference of air and ground wave. It is also clear to see that there is a lot more present at that location besides

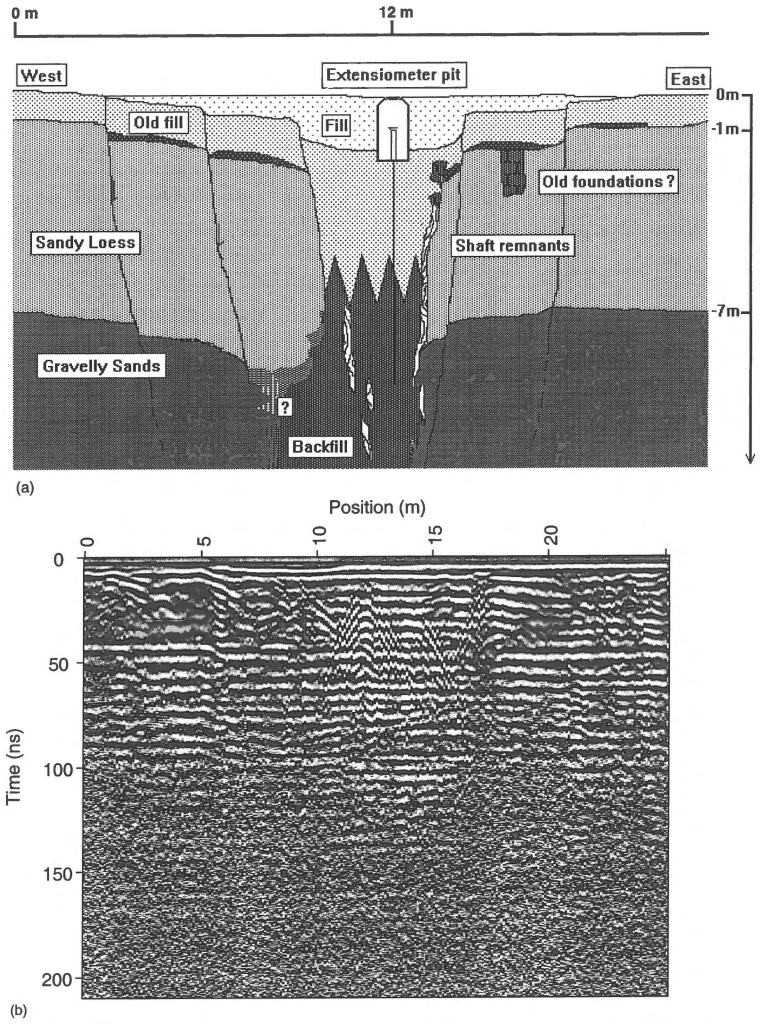

Figure 13. The cross-section model of the investigated Limburg mineshaft (a) and the corresponding common-offset measurement obtained with a 225 MHz shielded antenna system (b). The extensiometer pit at 12 m is clearly visible in the radar section as a hyperbolic event just before 20 ns. Shallow fractures at 2, 6 and 17 m due to saggings are also visible in the radar section, while those drawn in (a) are only visible in the radar section by a one sided-slope of a hyperbola.

the steel plate. This can be due to inhomogeneities in the subsurface. A common problem here is to distinguish between the signal from these inhomogeneities and that from the buried object to be detected.

Another aspect in the choice of antennas for a survey is the penetration depth for different frequencies. It is observed that only noise is present for f_c = 900 MHz and $t > 30$ ns, while there are still reflections visible for f_c= 450 MHz and $t > 30$ ns (Figure 12). Also the wavelength compared with the dimension of an object has its influence on the detectability of the object. Objects that are small compared to the wavelengths of the applied field and that show a small contrast in the electromagnetic properties to their surroundings, remain invisible. So the choice of the antennas for the detection of objects is a trade off between higher detectability but lower penetration depth with higher-frequency antennas, and lower detectability with higher penetration depth with lower-frequency antennas.

Detection of an abandoned mine shaft

In the Limburg coal field (the Netherlands) an old coal mine has been secured. Several sagging fractures have been investigated in the past (Lengemann 1996). A cross-section is depicted in Figure 13a. After renovation the location has been investigated using

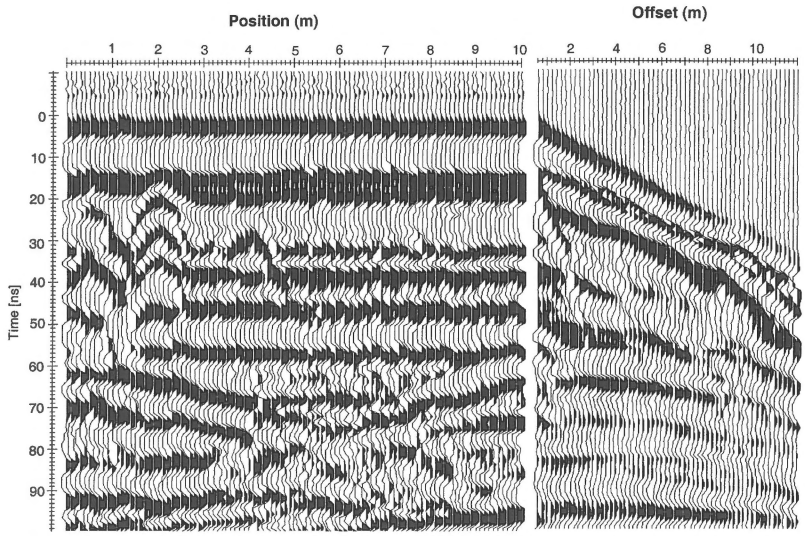

Figure 14. A common-offset (left) and CMP (right) measurement combined in display such that hyperbolas in the common-offset section are easily detected in the CMP section as above-surface reflections by their small temporal move-out as a function of offset. This example is from a 200 MHz unshielded antenna system. The steeply dipping slopes of the hyperbolas at 2 and 4 m from the starting point in the common-offset section indicate the presence of buried pipes.

different frequencies and different antenna systems (Mooijman 1997). In this particular environment we employed shielded antennas because the presence of many obstacles above the surface would otherwise cause too much interference. The results of this measurement, using a center frequency of 225 MHz, are depicted in Figure 13b. The velocity obtained with a CMP measurement is 0.1 m/ns (propagating wave regime). The extensiometer pit at position 12 was clearly visible as a hyperbolic event. Also the effect of several fractures due to the saggings can be distinguished in the data at positions 6 and 17, and possibly at 2, 10 and 14 m.

Detection of buried pipes in a conductive environment

Measurements have been carried out to detect pipes in the subsurface of Delft. An unshielded antenna with a center frequency of 200 MHz is used. The subsurface at this location is a conductive embedding due to the presence of clay, and a joint diffusion and wave propagation is expected, not ideal for a GPR survey. The results are depicted in Figure 14 with on the left a common-offset section with maximum position at 41 m, and on the right the CMP result with the location of 41 m as fixed midpoint between source and receiver. In the CMP results we can observe the air wave and also the ground wave in the first seven traces. Using Equation (6) the velocity of the ground wave can be derived as 0.08 m/ns. It is further observed that the first positive amplitude ($t = 0 - 5$ ns) is part of the air wave, but the second positive amplitude ($t = 14 - 20$ ns) is a combination of the air wave and the ground wave. At positions 2 and 4 m from the starting point in the common-offset section, objects are clearly indicated by the hyperbolas. When we derive a velocity using Equation (7) for reflections for $t > 60$ ns we obtain very large values. This indicates that these events are reflections of objects present above the surface, in our case trees. No clear reflections from buried layers or objects can be detected in the result of the CMP measurement.

Detection of ground-water level in sand dunes

In a low-loss environment (propagating wave regime), the sand dunes along the North Sea coast of the Netherlands, measurements have been carried out with three different center frequencies, f_c = 110, 225 and 450 MHz (Figure 15). The event at about 50 ns visible for all three frequencies can be recognized as the ground-water level. An overview of typical radar-stratigraphic features that are characteristic for the environments of the Netherlands can be found in Van Overmeeren (1996).

At a low frequency a low resolution and only horizontal reflections are visible. Eastward dipping layered structures can be recognized at the high fre-

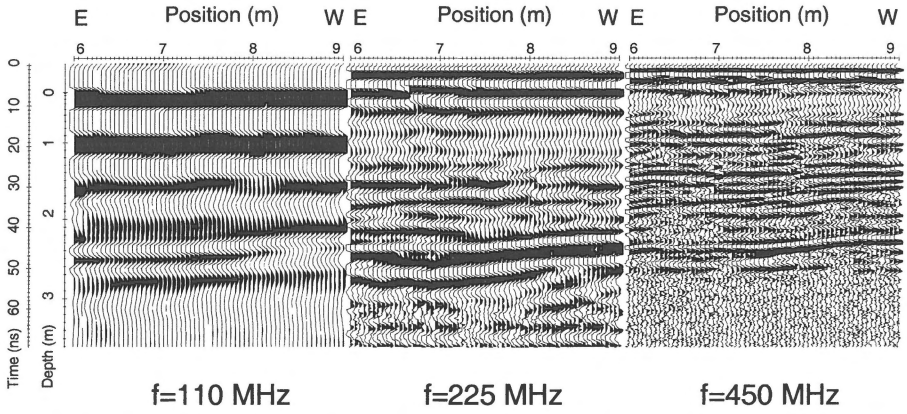

Figure 15. Comparison of data obtained from one single survey line with three different antenna systems in terms of their center frequencies. The level of detail clearly increases with increasing frequency of the antenna system, while the depth of penetration of the 900 MHz antenna (right) is clearly less than that of the 450 MHz antenna (middle). The 225 MHz antenna is not very useful in this sand-dune environment to distinguish different reflectors in the first two meters because the direct air and ground waves interfere and have a high amplitude masking the shallow subsurface reflectors.

quency of 450 MHz. The ultimate goal would be to be able to combine these data sets in a structured approach into a subsurface image. The data cannot simply be added and different kinds of amplitude and time-scaling approaches have failed to produce a single coherent image. However, it is evident that an increasing level of detail is obtained when a higher center frequency is used.

Conclusions

It has been shown that the commonly used scalar far-field approximation is valid for describing electromagnetic propagation and reflections for most materials for frequencies above 200 MHz. For resistive materials this is already the case at lower frequencies. This approximation is, however, not valid to describe propagation and reflection of electromagnetic waves emitted and recorded by finite-length electric dipoles.

The detection of an object by GPR depends on many factors, e.g. the contrast between the properties of the object and its embedding, the frequencies of the applied field and the depth of the object. For example the detection of the ground-water level is usually very simple because it is a strong reflector. Also the properties of the embedding have a great influence, especially regarding velocity and attenuation dispersion depending on the frequency range of the antennas used. Simple data analysis can be used effectively for the detection and location estimation of high-contrast reflectors and scatterers. It is not effective for low-contrast scatterers or scatterers in the presence of high-amplitude clutter. Then more sophisticated processing techniques should be used. These are currently under development.

Different antennas should be used to cover a wide frequency band and it is difficult to combine data from these antennas from the same subsurface. This scaling deserves further investigation.

References

Annan, A.P. 1996 Transmission dispersion and GPR – J. Environm. Engin. Geophys. 22: 125–136

Davis, J.L. & A.P. Annan 1989 Ground-Penetrating Radar for high-resolution mapping of soil and rock stratigraphy – Geophys. Prospecting 37: 531–551

De Hoop, A.T. 1995 Handbook of radiation and scattering of waves. Academic Press, London, 1085 pp

Felsen, L.B. & N. Markowitz 1994 Radiation and scattering of waves. IEEE-Press, New York, 888 pp

Fisher, E., G.A. McMechan, A.P. Annan & S.W. Cosway 1992 Examples of reverse-time migration of single-channel ground-penetrating radar profiles – Geophysics 57: 577–586

Goodman, D. 1994 Ground-penetrating radar simulations in engineering and archaeology – Geophysics 59: 224–232

Lengemann, A. 1996 Bericht über die Sicherung des Catharina Schachtes. Arbeitskreis 'Alte Schächte', Würselen, 7 pp

Mooijman, O.P.M. 1997 Detecting Abandoned Mineshafts in the Limburg Coal Field – MSc Thesis Delft University of Technology, Faculty of Applied Earth Sciences, No. 152, 80 pp

Turner, G. 1994 Subsurface radar propagation deconvolution – Geophysics 59: 215–223

Van Overmeeren, R.A. 1996 Radar facies of unconsolidated sediments in the Netherlands – A radar stratigraphic interpretation method for hydrogeology. 6th Int. Conf. Ground Penetrating Radar (GPR'96), Sept. 30–Oct. 3, Sendai, Japan: 167–172